Observations of Upper Ocean Temperature and Salinity Structure During the POLE Experiment

JAMES J. SIMPSON[1] AND CLAYTON A. PAULSON

School of Oceanography, Oregon State University, Corvallis 97331

(Manuscript received 4 September 1978, in final form 19 March 1979)

ABSTRACT

Mid-ocean observations (35°N, 155°W) of temperature and salinity were made from *R/P Flip* during the period 28 January–14 February 1974 as part of the NORPAX POLE Experiment.

Autocorrelations for the time series of depth of several σ_t surfaces confirm the presence of a semi-diurnal internal tide whose amplitude is about 10 m. The period of 12.7 h determined from the autocorrelation analysis is not statistically significantly different from the period of the M2 semidiurnal tide (12.4 h). The coherence between pairs of time series of the depth of the σ_t surfaces is high, ranging from 0.97 to 0.91 at the frequency of the peak in the spectrum corresponding to the semi-diurnal tide. The coherence between a given σ_t surface and deeper lying surfaces decreases slowly with the mean separation between surfaces. The vertical coherence scale suggests that most of the energy of the semi-diurnal internal tide is in the low-order modes. The data show that the phase difference between surfaces increases with the mean separation between surfaces at the approximate rate of $+35°\ (100\ \text{m})^{-1}$. Estimates of the vertical and horizontal wavelengths of the observed semi-diurnal internal tide are 1 km and 35 km, respectively.

One-dimensional mixed-layer deepening models fail to predict the mixed-layer depths and temperatures observed during POLE. Horizontal advection, as evidenced from the salinity maximum frequently occurring at the bottom of the mixed layer and other near-surface changes in salinity and temperature not associated with local surface forcing, are responsible for the failure. During the one period in which the one-dimensional models may be applicable a value of the mixing energy flux coefficient $m = 0.0017$ was obtained.

1. Introduction

Temporal variations in upper ocean temperature and salinity structure are caused by the exchange of energy, momentum and mass across the air-sea interface and by advection. To better understand upper ocean processes and evaluate existing parameterizations of such processes, the POLE Experiment, a component of the North Pacific Experiment (NORPAX) was conducted during the period 28 January–14 February 1974.

The experimental site (near 35°N, 155°W) is shown in Fig. 1. The North Pacific Current dominates the general circulation of this region. The observational area lies in the transition zone between the trade winds to the south and the westerlies to the north. Large-scale changes in the curl and divergence of the wind stress and in the exchange of heat and mass occur in such a region. Superimposed on this flow are several other features which complicate the hydrodynamics of the region. The subtropical front is known to meander, in the mean, between 31° and 33°N (Roden, 1974). Observations (Roden, 1970, 1972) suggest that in winter the horizontal temperature and salinity gradients contribute approximately equally to the density gradient, while in summer the temperature gradient weakens. The horizontal salinity gradient appears to remain about the same throughout the year. The region of the trade winds northeast of the Hawaiian Island Chain has upward fluxes of latent heat in excess of 9.8 mW cm^{-2} over a 24 h period. This leads to the formation of a high-salinity Subtropical Water Mass which contrasts markedly with the less saline eastern Pacific Central Water characteristically found north of 35°N. This saline subtropical water can penetrate to depths as great as 200 m (Reid, 1965; Seckel, 1968).

The purpose of this paper is to report observations of temperature and salinity obtained during a 15-day period of intensive sampling from *R/P Flip* as part of the NORPAX POLE Experiment and to interpret these observations in terms of physical processes, both local and advective, which might explain the observed structure.

2. Observations

Vertical profiles of temperature and salinity were taken from *R/P Flip*, [Floating Instrument Platform (Bronson and Glosten, 1968)] throughout

[1] Present affiliation: Scripps Institution of Oceanography, La Jolla, CA 92093.

0022-3670/79/050869-16$08.00

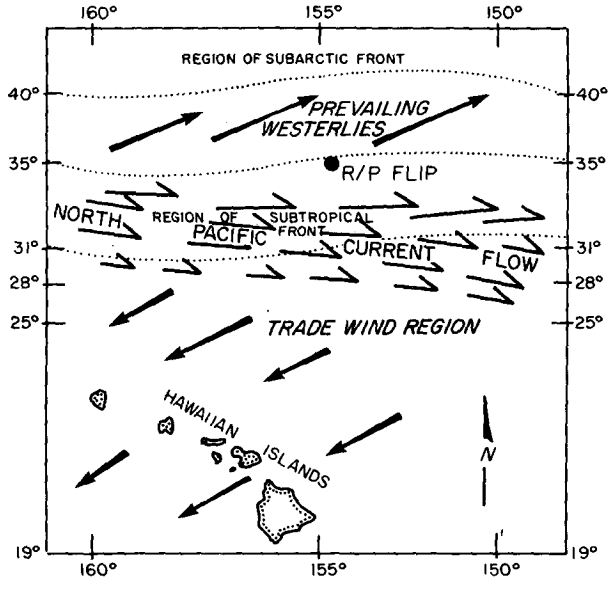

FIG. 1. The POLE Experiment was conducted in the central North Pacific approximately 800 miles north of the Hawaiian Islands. *R/P Flip* occupied a station centered around 35°N, 155°W. The region is hydrographically complex.

the period 30 January–14 February 1974, approximately 800 mi north of the Hawaiian Island Chain under free drift conditions. *Flip* is a large manned spar buoy with approximately 90 m of its 130 m length submerged, resulting in a high degree of stability. Typical heave amplitudes were about 10 cm, while pitch and roll amplitudes were usually less than 2°. The position of *Flip* ranged from 35°39′ to 34°36′N and from 155°05′ to 155°25′W. Profiling was concentrated in the surface layer and thermocline. The maximum depth reached was 325 m. On average, eight profiles were measured per day. On occasion, more intensive sampling was maintained.

In addition to profiles of temperature and salinity, measurements of atmospheric radiation (Simpson and Paulson, 1979a) and oceanic irradiance (Paulson and Simpson, 1977) were made. Sea surface temperature was measured with a Barnes Engineering Company PRT-5 radiation thermometer (Simpson and Paulson, 1979b). Standard cup anemometers were used to measure wind speed. Dry- and wet-bulb temperatures were measured approximately hourly by use of a ventilated psychrometer. Bucket temperatures were recorded at the same time. Estimates of wind stress and latent and sensible heat flux were obtained by use of the standard bulk formula. The exchange coefficient used was 1.4×10^{-3}. Hourly values of observed and derived quantities are shown in Fig. 2. These values were obtained by interpolating between observations using a cubic spline.

Direct measurements of the latent and sensible heat flux, using the eddy correlation technique, were made (Friehe and Schmitt, 1976). The variability of the near-surface currents was observed with a vertically profiling current meter system and with drogues (Davis *et al.*, 1978).

3. Instrumentation

A Bissett-Berman Model 9040 Salinity/Temperature/Depth (STD) Measuring System was used as the profiling device. Temperature is determined with a platinum resistance thermometer having a time constant of 0.35 s, according to the manufacturer. Salinity is determined from simultaneous measurements of conductivity, temperature and depth. The time response of the conductivity probe is 10 ms. Unfortunately, conductivity is not the recorded variable. Rather, the instrument internally compensates for the effects of temperature and pressure and gives a direct estimate of salinity. Accuracies for depth, temperature and salinity are 1 m, 0.01°C and 0.03‰, with corresponding resolutions of 0.2 m, 0.005°C and 0.01‰. Data were recorded in digital form with a sampling rate of 5 Hz.

Temperature was standardized against a Mueller platinum resistance bridge. Salinity was standardized with reference to surface samples taken during each profile. A Bisset-Berman Model 6230 inductive salinometer was used to determine the salinity of the surface samples. This device can accurately resolve salinity to within 0.003‰.

A correction was applied to the depth signal to eliminate the effect of ambient atmospheric pressure. Corrections due to platform motion were unnecessary, as the amplitude of *Flip*'s vertical oscillations is typically 10 cm.

Spectral analysis of GATE B-scale data, taken with Bisset-Berman Model 9040 STD's, suggests that a large percentage of the variance associated with the pressure signal is contributed at frequencies >0.67 Hz. This variance is thought to be internal system noise (Elliot, 1975). The GATE results suggest that a low-pass filter is required to attenuate signals above 0.67 Hz. A two-stage running mean filter, designed by Holland (1968), was used.

Differences in the time constants of the temperature and salinity sensors introduce errors in the observed values of temperature and salinity. To correct the temperature signal for the thermal inertia of the sensor, a local temperature gradient was calculated from a 12-point, noncentered, linear regression. The center of the regression is 0.3 s ahead of the point to be corrected. The corrected temperature T_c is then given in terms of the uncorrected temperature T_o, i.e.,

$$T_c = T_o + \gamma \frac{\Delta T_o}{\Delta t}, \qquad (3.1)$$

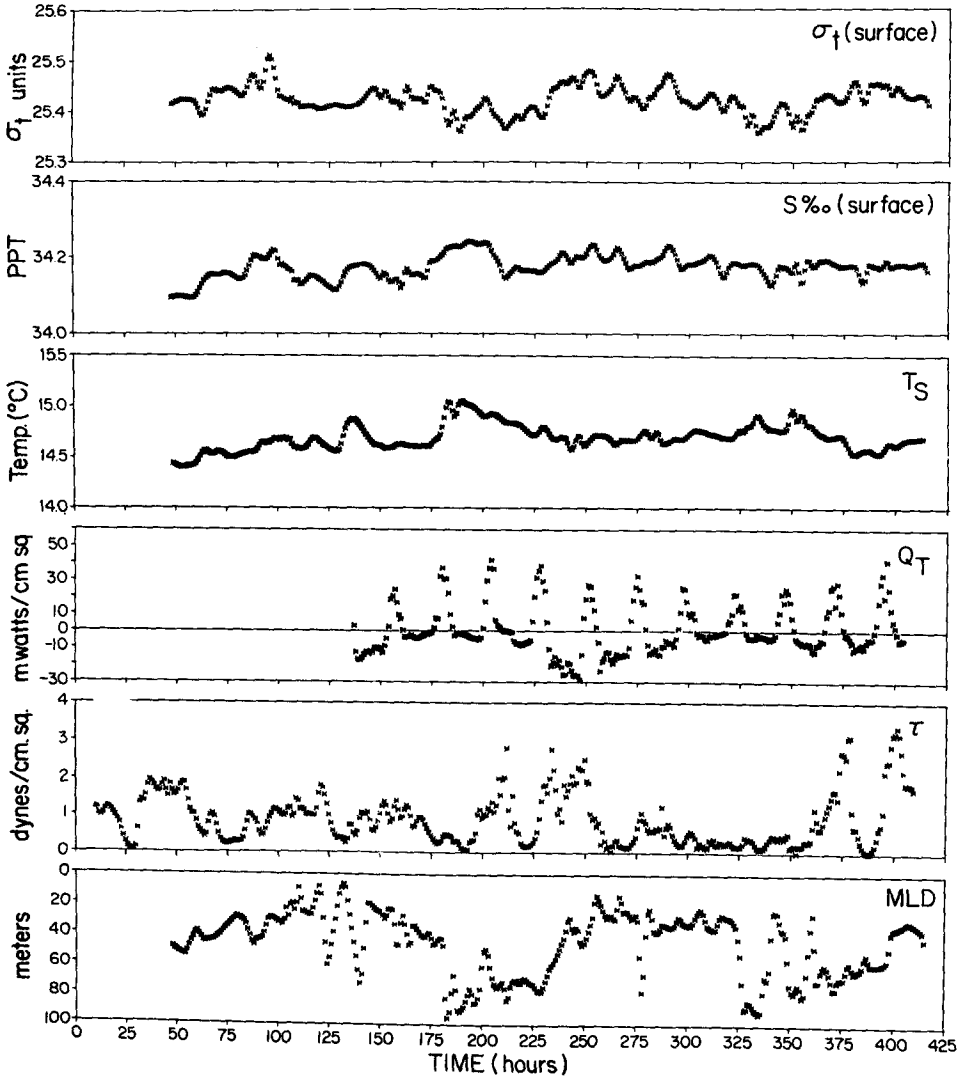

FIG. 2. Hourly values of the surface σ_t, surface salinity, sea surface temperature, total heat flux at the surface Q_T, wind stress τ, and the mixed-layer depth MLD. Hourly values were obtained by interpolating between observations using a cubic spline. The origin of the abcissa is 1000 GMT 28 January 1974.

where γ is the response time of the temperature sensor.

The salinity correction is based on a relation (Mosetti, 1967) between the conductivity C and the measured temperature and salinity T_o and S_o:

$$C = (\Gamma + \mu T_o^k) S_o^h, \tag{3.2}$$

where $\Gamma = 1.17013$, $\mu = 0.03299$, $k = 1.05257$ and $h = 1.10807$. As this relation is assumed to hold for both corrected and measured values, the correction factor assumed the form

$$\lambda = \left(\frac{\Gamma + \mu T_o^k}{\Gamma + \mu T_c^k}\right)^{-h}. \tag{3.3}$$

The corrected salinity S_c, specified in terms of the observed salinity S_o, then assumes the form

$$S_c = S_o[(\lambda - 1)\xi + 1]. \tag{3.4}$$

This relation reduces to the correction used by Elliot (1975) for the case $\xi = 1$. The factor ξ is introduced to minimize the cumulative magnitude of the inversions in the density profiles determined from the corrected profiles of temperature and salinity. Observations of density inversions are most likely introduced by erroneous salinity measurements made in the presence of sharp temperature gradients. Occasionally, turbulence in the water may cause real density inversions which can persist only for brief periods. The corrected salinity was low-pass filtered, in a manner analogous to pressure. Numerous numerical experiments indicated that the observed density inversions were minimized with $\xi = 6$. The resulting triplets (T_c,

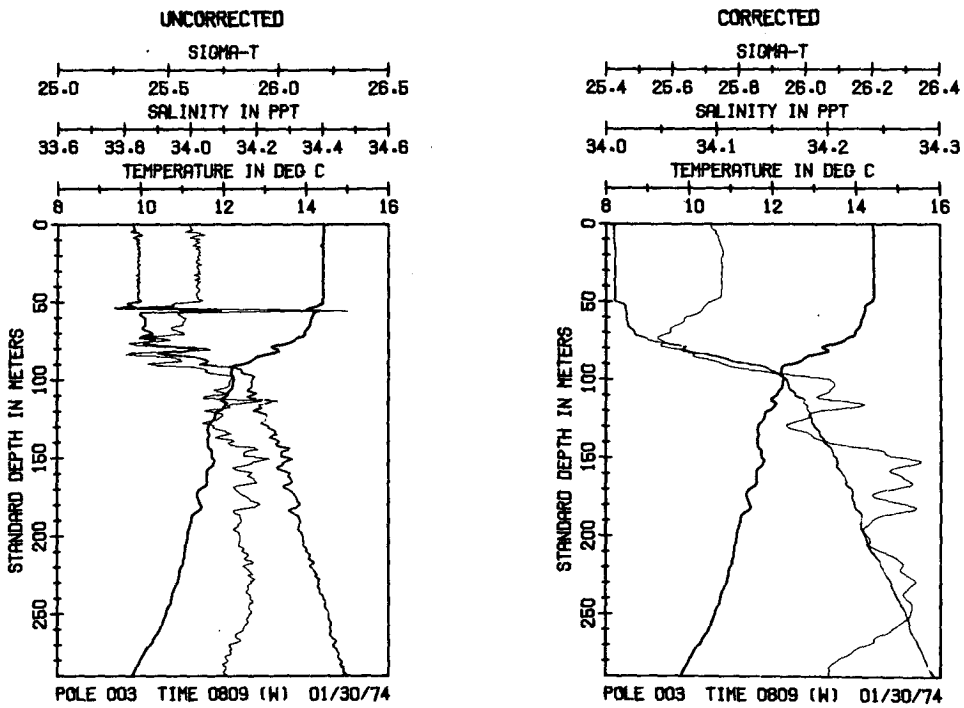

FIG. 3. Examples of uncorrected and corrected temperature, salinity and density profiles for a typical hydrocast. Corrections were made for the difference in the time response of the conductivity and temperature sensors.

S_c,D) were averaged over 1 m intervals, and standard depth values computed by interpolation from the averaged data sets. The σ_t profiles were computed using a series expansion in terms of the corrected temperature and salinity (Fofonoff and Tabata, 1958; Sweers, 1971). In Fig. 3 uncorrected and corrected profiles of temperature, salinity and σ_t are shown for a typical observation. A data report summarizing all the STD observations has been prepared (Simpson and Paulson, 1977).

4. Surface conditions

a. Surface wind stress

The observational period was characterized by low wind speeds. The wind stress, calculated from the bulk formulas with a drag coefficient of 1.4×10^{-3}, has a mean value of 0.66 dyn cm^{-2} (10 dyn cm^{-2} = 1 Pa). For one 3-day period the wind stress is considerably less than 0.5 dyn cm^{-2}. From Fig. 2 it is evident that only two periods of relatively high winds occurred during the experiment: one near the center of the experiment with a maximum wind stress of 2.7 dyn cm^{-2} and the other at the end of the experiment with a maximum wind stress of 3.3 dyn cm^{-2}.

b. Surface heat flux

The net all-wave and longwave radiative fluxes were measured with a Swissteco Pty. Ltd. MS-1 net radiometer and a Middleton Instruments net longwave radiometer, respectively. The net all-wave radiative flux includes radiation in the bandwidth 0.3–60.0 μm. The net solar flux was measured with Eppley radiometers. The latent and sensible heat fluxes were determined from standard meteorological observations, using the bulk formulas and a drag coefficient of 1.4×10^{-3}. The total heat flux Q_T was computed from these observations. The sea surface temperature was constructed by extrapolating the 1 m temperature values, measured with the STD, to the surface. Hourly values (shown in Fig. 2) of these surface variables were obtained by interpolating between observations with a cubic spline.

The net all-wave flux dominated the surface heat balance for most of the experiment. However, midway through the experiment enhanced surface cooling occurred. An increase in wind speed during this period resulted in a large latent heat transfer. The sensible heat flux never exceeded ± 2.0 mW cm^{-2} (1 mW cm^{-2} = 10 W m^{-2}) and typically was less than ± 1.0 mW cm^{-2}. Friehe and Schmitt (1974) computed average values of the latent and sensible heat fluxes for the 17 days of observations. They found that the sensible heat flux was two orders of magnitude less than the latent heat flux for this period. They report an average Bowen ratio of 0.013, substantially less than the commonly used value of 0.1.

TABLE 1. Daily heat flux budgets for the POLE experiment computed symmetrically about local solar noon. All units are in mW cm^{-2} and represent average values over a 24 h period. Heat gain by the ocean is assumed positive.

Date February 1974	Total heat flux	Radiative heat flux	Turbulent heat flux
3	−1.1	5.1	−6.2
4	6.3	7.0	−0.7
5	6.1	6.7	−0.6
6	−0.5	5.1	−5.6
7	−8.9	7.6	−16.5
8	−2.3	6.3	−8.6
9	2.2	4.0	−1.8
10	3.3	4.4	−1.1
11	2.4	5.7	−3.3
12	2.3	4.5	−2.2

A daily heat budget is given in Table 1. Heat gain by the ocean is taken positive. Daily flux values were calculated as a centered average about local solar noon (time zone W).[2] These results indicated that the ocean gained heat for six days, was in near-thermal equilibrium with the atmosphere for two days, and lost heat for two days. These results, coupled with the observed low wind stress, indicate that upper ocean dynamics might have been dominated by net surface heating for a part of the experiment.

[2] W time = GMT − 10 h.

c. Mass and buoyancy flux

Only one period of intense precipitation occurred during the experiment. Overall, evaporation and precipitation were in near equilibrium, with precipitation exceeding evaporation by 23 mg cm^{-2}.

At the surface the buoyancy flux M_0 is determined by air-sea transfer (Dorrestein, 1979)

$$M_0 = g\rho^{-1}[\beta Q_T c_p^{-1} + \kappa S(R - E) + \beta \Delta T R], \quad (4.1)$$

where g is the acceleration due to gravity, ρ the density of seawater, β the thermal coefficient of expansion for seawater, Q_T the total heat flux at the surface, c_P the specific heat of seawater at constant pressure, κ the saline coefficient of contraction, S the surface salinity, E and R are the evaporation and precipitation rates, respectively, and ΔT is the difference in temperature between the precipitated water and the surface water. Mass gain by the ocean is positive. Hourly values of the surface temperature, salinity and density are shown in Fig. 2. These time series show the expected diurnal variation associated with daytime heating and nighttime cooling. Overall, the mass flux at the interface had little influence on the buoyancy flux, except possibly during one brief period of precipitation which occurred near midnight on 5 February

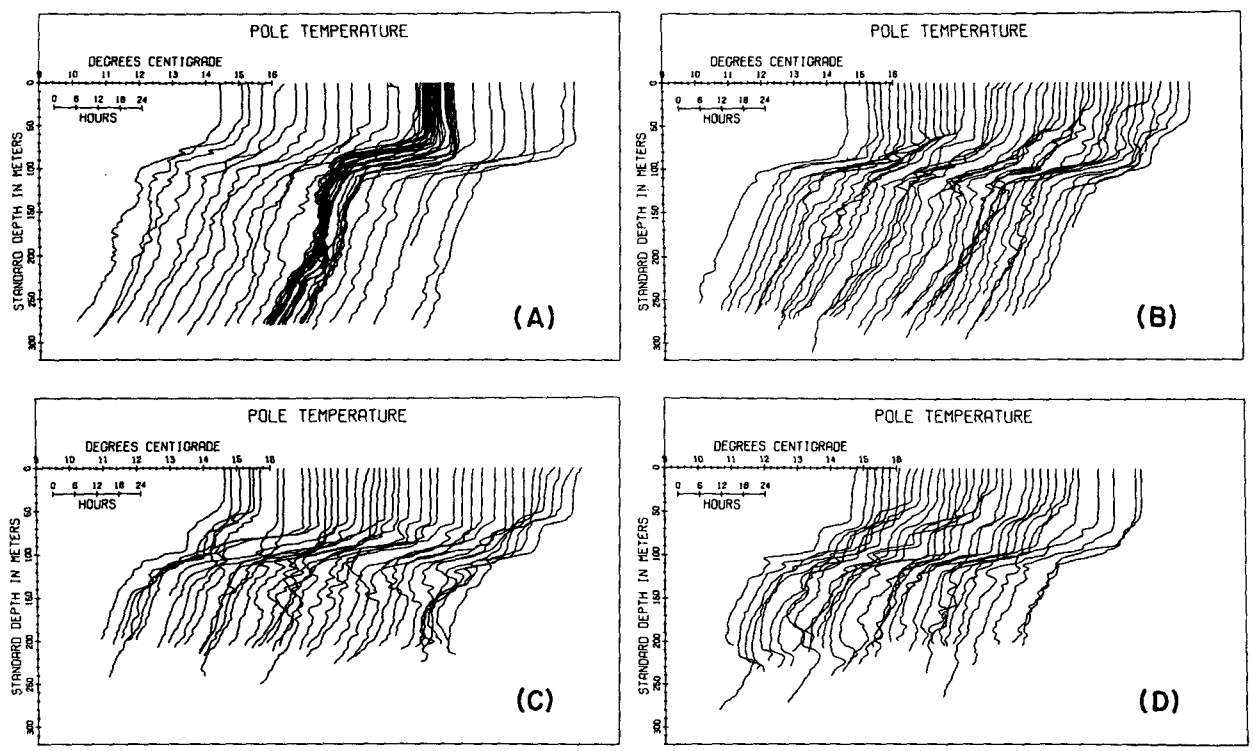

FIG. 4. Profiles of temperature taken during the experimental period. The spacing between adjacent profiles is proportional to the time difference between hydrocasts.

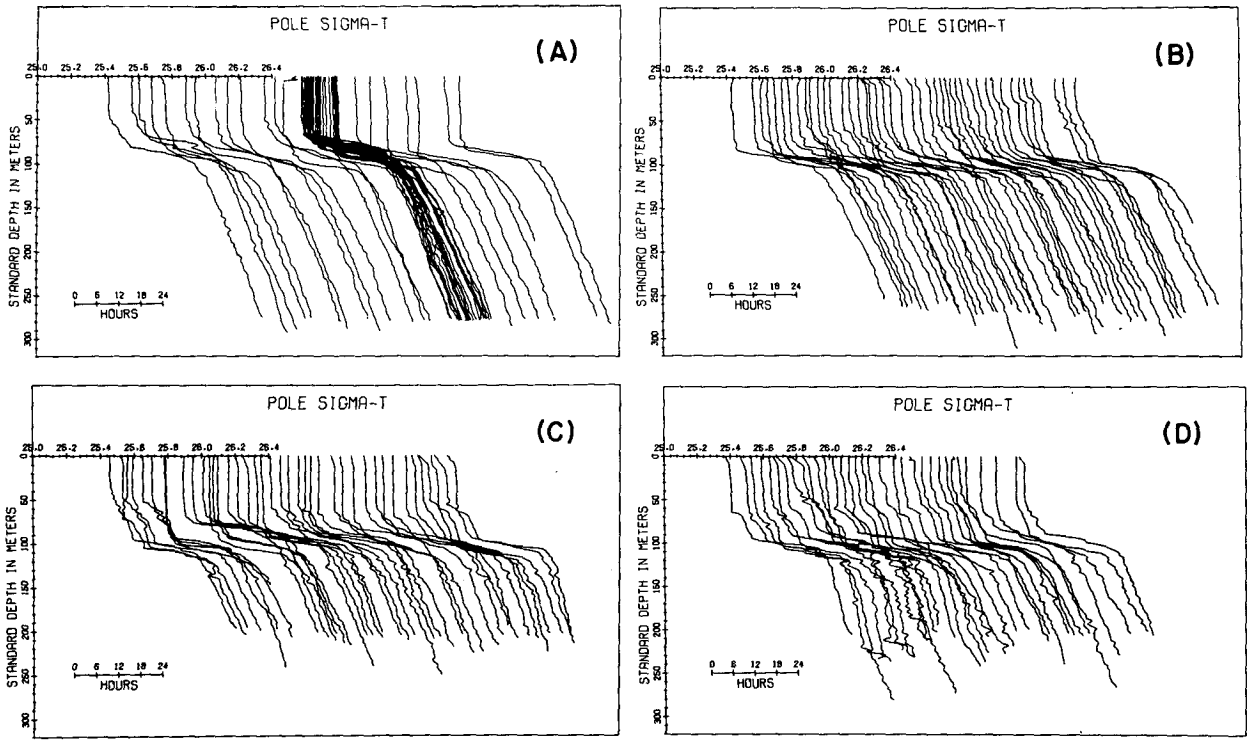

FIG. 5. Profiles of σ_t taken during the experimental period. The spacing between adjacent profiles is proportional to the time difference between hydrocasts.

(Simpson, 1977). The net heat flux at the surface dominated the buoyancy flux throughout the experiment.

5. The surface layer

Profiles of temperature and σ_t for the entire experiment are shown in Figs. 4 and 5, respectively. The spacing between adjacent profiles is proportional to the time interval between measurements. The seasonal thermocline is at a depth of ~100 m. However, for large periods of time the layer above the seasonal thermocline is far from well mixed. Temperature inversions are frequently seen at the base of the mixed layer. These inversions are compensated by observed salinity maxima so that the density profile is stable. Steplike structure and multiple isothermal layers frequently form in the surface layer during periods of low winds and net heat gain at the surface. During subsequent, though brief, periods of high winds these features are eroded quickly. Comparison of the temperature and σ_t profiles indicates that the density structure was determined principally by temperature.

The well-mixed layer usually consists of the upper 10 to 100 m of the ocean, is characterized by nearly uniform density structure, and responds directly to atmospheric forcing for time scales greater than an hour. The mixed-layer depth, shown in Fig. 2, is defined as the shallowest depth at which the density is not more than 0.02 σ_t units less than the density at a depth of 5 m. Diurnal variations in mixed-layer depth resulting from local surface processes are evident. The low wind speeds and positive total heat fluxes, which characterized the POLE Experiment, favored the formation of warm shallow surface layers of nearly uniform density, shown in Fig. 4. Such features persisted until periods of sustained high winds occurred, whereupon the depth of the mixed layer was reestablished between 50 and 60 m.

The only significant departures from this pattern occurred midway into and at the end of the experiment. The period 6–8 February is marked by intermittently high wind stress (frequently >2.5 dyn cm^{-2}) and enhanced evaporative and net longwave heat fluxes. These processes combined to produce the period of sustained deepening shown. Initially, high wind stress (τ = 2.9 dyn cm^{-2}) resulted in a period of rapid deepening during the 15 h interval beginning 200 h after the initiation of observations. A subsequent quiescent period ($\tau \leq 0.5$ dyn cm^{-2}) allowed for the quick reestablishment of a warm, light surface layer. During the interval 230–270 h into the experiment, sustained winds again occurred ($\tau > 2.0$ dyn cm^{-2}) and the rapid and sustained deepening shown in Fig. 2 followed.

Contours of σ_t for the observational period are shown in Fig. 6. The scale at the base of the figure

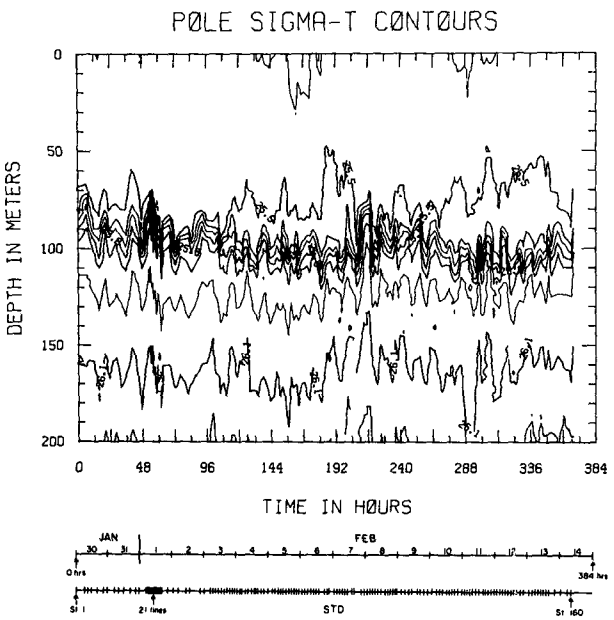

FIG. 6. The isopycnal distribution observed during POLE. The contour interval is 0.1 σ_t units. The σ_t surfaces show strong semi-diurnal variation in vertical amplitude about their mean position.

indicates the time at which a given STD profile was made. Convergence of the isopycnals between 50 and 80 m occurs during periods of high winds. The isotherms behave in a similar fashion. This feature is absent in the isohaline contours (Simpson, 1977), suggesting that the temporal variations in the density structure of the upper 100 m are due primarily to thermal processes.

During periods of calm winds, a warm surface layer, corresponding to the 25.4 isopycnal, formed rapidly. Thus, for part of the observational period the ocean gained heat due to surface processes, acting on diurnal time scales or longer, and intermittently took on some of the characteristics of a summertime well-mixed layer. These observations are consistent with those of Barnett (1976), who found that the total heat content down to a depth of 300 m along a 170°W section at approximately 30°N was slightly greater in February than in January.

6. The subsurface layer

Time series of depth for selected σ_t surfaces occurring at a depth below 60 m are shown in Fig. 7. All the time series show a strong semi-diurnal variation in vertical amplitude about their mean position. These time series correspond to σ_t surfaces of 25.6, 25.9, 26.0 and 26.1 and occur at mean depths of 92.1, 106.3, 124.7 and 163.2 m, respectively. The first four central moments for each time series are given in Table 2. The upper three σ_t surfaces all have a positive skewness ranging from 0.43 (σ_t = 25.6) to 0.33 (σ_t = 26.0). Only the deepest surface (σ_t = 26.1) has a slightly negative skewness, $s = -0.04$. The positive skewness of these records suggests they are similar to surface gravity waves.

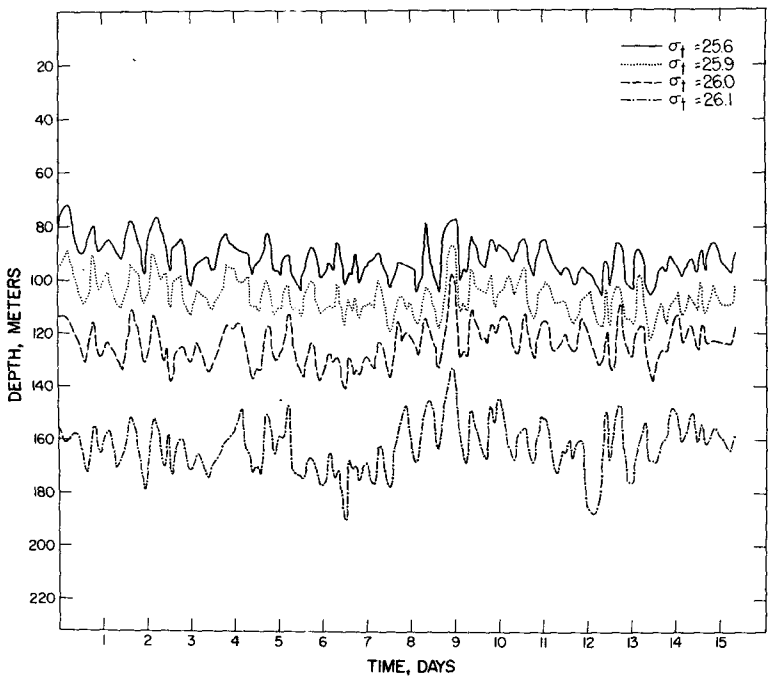

FIG. 7. Time series of depth of four σ_t surfaces occurring below 60 m. The time series correspond to the 25.6, 25.9, 26.0 and 26.1 σ_t surfaces at mean depths of 92.1, 106.8, 124.7 and 163.2 m, respectively.

TABLE 2. Statistical parameters for the σ_t surfaces shown in Fig. 7. The skewness S and kurtosis K are normalized by σ^3 and σ^4, respectively, where σ is the standard deviation.

σ_t	Mean depth (m)	Standard deviation (m)	S	K
25.6	92.1	6.9	.43	2.97
25.9	106.8	6.6	.46	3.05
26.0	124.7	6.9	.33	3.35
26.1	163.2	9.4	−.04	3.39

The kurtosis is close to 3 for all of the records suggesting the variations in amplitude of a given surface are nearly normally distributed. However, the kurtosis increases with depth, reaching a maximum value of 3.39 (σ_t = 26.1). This suggests that progressively deeper surfaces are less well-approximated by a normal distribution.

The autocorrelation function of a signal $u(t)$ having zero mean is

$$\Phi(\tau') = \frac{\overline{u(t)u(t')}}{\overline{u^2}}, \qquad (6.1)$$

where the time difference $\tau' = t' - t$. It provides a measure of the time interval over which $u(t)$ is correlated with itself. Autocorrelations for the four σ_t surfaces are shown in Fig. 8. The unit of lag is 14.36 min, and the length of the series is 15.5 days. Several features are evident from these autocorrelations. The autocorrelation function, characteristic of turbulent processes, is well damped, may become slightly negative after a few lags and then rapidly approaches zero. This insures that the integral scale for the turbulent process is small. By contrast, the autocorrelation function for each of the σ_t surfaces in Fig. 7 shows an oscillatory behavior, remaining highly coherent for a period of 2 days or longer. The oscillatory pattern shown in Fig. 8 has a period of 12.7 h. This period is not statistically significantly different from the semi-diurnal M2 tidal period of 12.4 h (Defant, 1961). This suggests the presence of a semi-diurnal internal tide.

A frequency spectrum for each of the four σ_t surfaces is shown in Fig. 9. Most of the variance occurs at periods corresponding to the semi-diurnal period or longer. Considerable energy occurs at the inertial period; for a latitude of 35° the inertial period T_p corresponds to 20.8 h. For periods less than the semidiurnal period, the spectrum falls off rapidly.

Phase and coherence spectral estimates were calculated for the various combinations of σ_t surfaces. These spectra are shown in Figs. 10 and 11, respectively. The values of the coherence and phase at the frequency corresponding to the peak in the coherence spectrum for each pair are given in Table 3. The peak in the coherence spectrum corresponds to a period of 11.5 h, close to the M2 semi-diurnal tidal period. The length of the time series prevents finer spectral resolution of the frequency scale. The coherence among all pairs is high, ranging from a maximum value of 0.97 for both the 25.6–25.9 and 25.9–26.0 pairs to a low of 0.91 for the 25.6–26.0 pair. The coherence between pairs of σ_t surfaces is shown as a function of the mean separation between surfaces in Fig. 12.

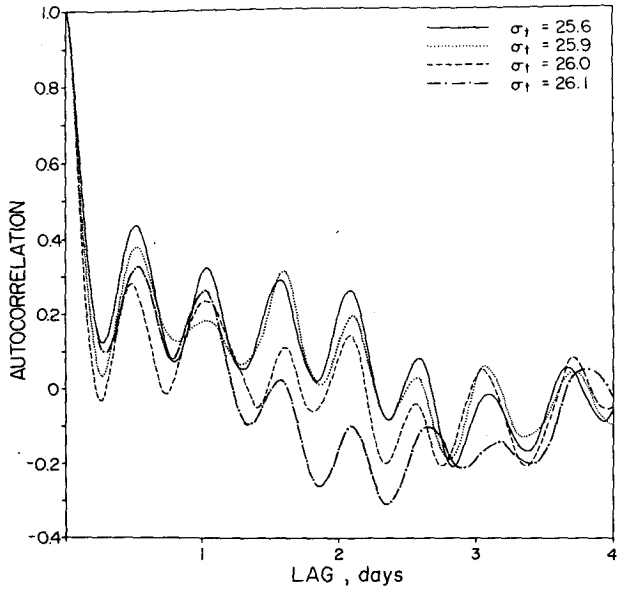

FIG. 8. Autocorrelation functions for the σ_t surfaces observed during POLE. The unit of lag is 14.36 min and the length of the series is 15.5 days. The period of the oscillation is 12.68 h, close to that of the semi-diurnal M2 tide, 12.42 h.

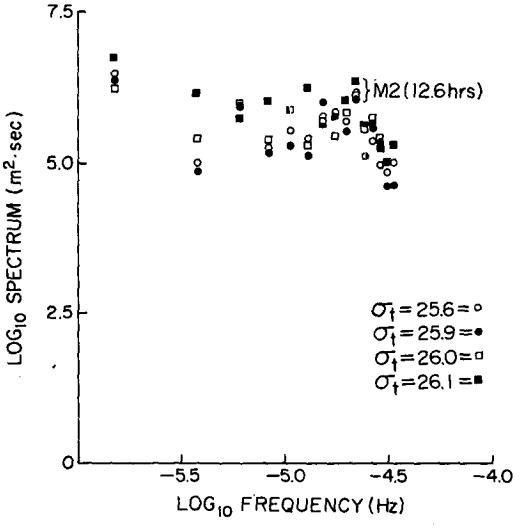

FIG. 9. Individual spectra for the four σ_t surfaces. The semi-diurnal spectral peak occurs at 12.6 h. For periods below the semi-diurnal, the spectra fall off rapidly.

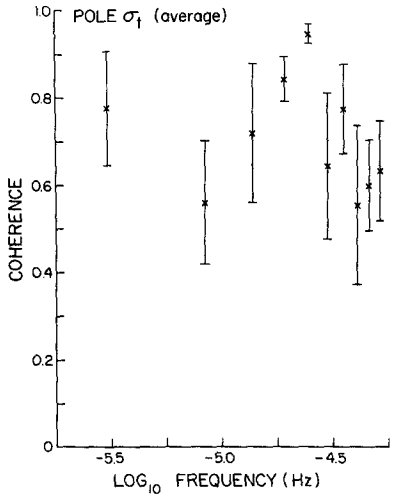

FIG. 10. Average coherence spectrum for the various combinations of σ_t surfaces. The error estimate is one standard deviation of the four band-averaged coherence spectra about the mean. A high coherence ($0.91 \leq COH \leq 0.97$) at the peak in the spectrum occurs for all pairs.

The coherence between a given σ_t surface and deeper-lying surfaces decreases slowly with the mean separation between surfaces. An estimate of the vertical wavelength λ_v of the semi-diurnal internal tide can be calculated from the coherence vs mean separation data by fitting the data to different types of curves. A parabolic least-squares fit of coherence as a function of mean separation between σ_t surfaces, forced through the point (0,1.0) suggests that an approximate length scale at which the coherence falls to zero is 170 m. Since this zero crossing corresponds to one-fourth the vertical wavelength, the estimate of λ_v obtained from the parabolic fit is 0.7 km. The uncertainty in this length scale is high. Data at depths >200 m were not routinely taken, hence the shape of the curve of the coherence vs mean separation is uncertain. The assumed parabolic dependence may be unrealistic. The same data fit to a cosine curve forced through the point (0,1.0) has a zero crossing at 180 m corresponding to a quarter-wavelength. This fit suggests that an estimate of the vertical wavelength is $\lambda_v \approx 0.7$ km, which is the same as the previous estimate. Parabolic and cosine fits without forcing the curves through the point (0,1.0) yielded estimates of $\lambda_v = 0.9$ and 1.2 km, respectively. For the calculations that follow a value of $\lambda_v \approx 1$ km is assumed. The vertical wavelength is approximately equal to one-third the total depth, implying third-order modal dynamics dominate the signal.

TABLE 3. Coherence and phase estimators for the σ_t surfaces shown in Fig. 7. Values correspond to the frequency at the peak in the coherence spectrum, 11.57 h.

σ_{t1}/σ_{t2}	Mean separation (m)	Coherence	Phase
25.6/25.9	16.8	0.97	−8
25.6/26.0	32.6	0.95	+3
25.6/26.1	71.1	0.91	+25
25.9/26.0	17.9	0.97	+11
25.9/26.1	56.4	0.93	+33
26.0/26.1	38.5	0.93	+22

The phase estimators between different σ_t surfaces, corresponding to the frequency of the peak in the coherence spectrum, are shown in Fig. 13 as a function of the mean separation between surfaces. The figure suggests that for a given σ_t surface, deeper lying surfaces lag the given surface by an amount dependent on the mean separation between surfaces. The only exception is the 25.6–25.9 pair for which the 25.9 surface leads the 25.6 surface by 8°. The data suggests that the phase difference increases with separation at the approximate rate of +35° $(100\ m)^{-1}$. This value yields an estimate of the vertical wavelength $\lambda_v = 1.2$ km which is consistent with our previous estimate. Deeper lying surfaces lagging shallower surfaces is consistent with upward energy propagation (e.g., Turner, 1973).

The dispersion relation for an internal wave under the assumption of a linear density gradient and the Boussinesq approximation (Turner, 1973) is

$$\omega = N\left(\frac{k^2}{k^2 + m^2}\right)^{1/2}, \qquad (6.2)$$

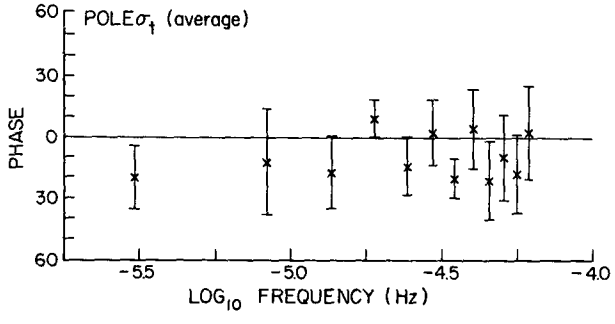

FIG. 11. Average phase spectrum for the various combinations of surfaces. The error estimate is one standard deviation of the four band-averaged phase spectra about the mean.

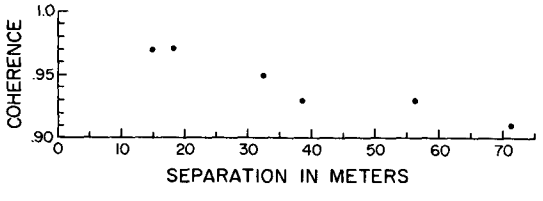

FIG. 12. Coherence as a function of mean separation between σ_t surfaces. An estimate of the vertical wavelength from the coherence vs depth data is $\lambda_v \approx 1$ km.

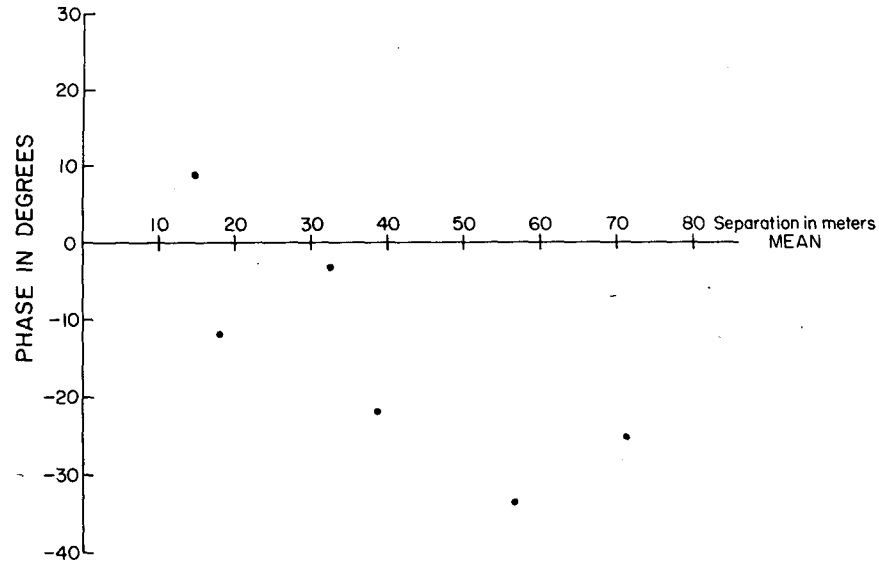

FIG. 13. The phase estimator at the frequency corresponding to the peak in the coherence spectrum as a function of the mean separation between σ_t surfaces. The data suggest that the phase difference between surfaces increases with the mean separation between surfaces at the approximate rate of $+35°$ (100 m)$^{-1}$.

where ω is the wave frequency, N the buoyancy frequency and k and m are the vertical and horizontal wavenumbers, respectively. The buoyancy frequency was determined from the observed density using the relation

$$N = \frac{g}{\bar{\rho}}\left(\frac{\partial \rho}{\partial z}\right)^{1/2}, \tag{6.3}$$

where g is the acceleration due to gravity, $\bar{\rho}$ the mean density and $\partial\rho/\partial z$ the observed vertical gradient of density. The buoyancy frequency at a depth of 145 m was calculated from the mean depths of the $\sigma_t = 26.0$ and $\sigma_t = 26.1$ surfaces. The mean separation between these surfaces is $\Delta z = 38.5$ m and the density difference is $\Delta\rho = 0.1 \times 10^{-3}$ g cm^{-3}. Thus, the buoyancy frequency is 2.9 cycles h^{-1}. The buoyancy frequency is the upper limit of frequency for which internal wave motions can exist in a stratified fluid. For low-frequency motions $k^2 \ll m^2$ and the dispersion relation simplifies. With $\omega = 1/12$ cph, $N = 3$ cph and $m = 1$ km^{-1} an estimate of the horizontal wavelength is $\lambda_h \approx 36$ km. For $N = 2.5$ cph, the horizontal wavelength is $\lambda_h \approx 30$ km. In making these estimates of the horizontal wavelength a value of the buoyancy frequency at shallow depth (145 m) was used since STD casts were not taken routinely at great depths. The buoyancy frequency may be smaller further down, say at 500 m, and a deeper value of N may be more appropriate since the vertical wavelength $\lambda_v \approx 1$ km. In the dispersion relation [Eq. (6.2)] effects of rotation were neglected. However, such effects would decrease the estimate of λ_h by no more than 20%.

Observations of the semi-diurnal internal tide in the central Pacific (42°N, 158°W) have been reported by Barnett and Bernstein (1975). Their observations suggest that the vertical displacement of isotherms is between 5 and 10 m, in good agreement with the presently reported results. The validity of Barnett and Bernstein's use of isotherms as a tracer of vertical water movement is degraded by the presence of weak temperature gradients and temperature inversions which frequently occurred in their data at the 100 m level. If one ignores the data at the 100 m level, the coherence between the 75 and 150 m levels is 0.84 and between the 50 and 150 m levels is 0.76 with phase shifts of $+4°$ and $+13°$, respectively. These values of coherence, while smaller than those presently reported, are in good qualitative agreement with our observations. The coherence between isotherms might be expected to be less than that between isopycnals because density is a better tracer of water motion than is temperature. The phase estimates of Barnett and Bernstein agree in sign and approximate magnitude with the observations reported here. Both sets of observations suggest that deeper-lying surfaces lag a given surface by an amount dependent on the mean separation between surfaces. This result is consistent with an interpretation of upward propagation of energy.

One may make an estimate of the horizontal wavelength of the semi-diurnal internal tide based on the phase difference between the moorings reported in Barnett and Bernstein (1975). They observed a coherence of 0.7 and a phase difference of 57° between temperature signals measured from two moorings

5.2 km apart. If one assumes that the wave crests were oriented perpendicular to the line between moorings, an estimate of the horizontal wavelength $\lambda_h = 33$ km is obtained [(360/57) × 5.2]. If, however, the wave crests were oriented at some angle θ to the line between moorings, the estimate of λ_h would be reduced. If it is assumed that waves from any direction are equally probable, then the estimate of 33 km must be multiplied by the absolute magnitude of $\sin\theta$ averaged over the interval $[0,\pi/2]$. Under this assumption $\lambda_h = 21$ km. These estimates are in fair agreement with values of λ_h determined from our measurements and Eq. (6.2). Barnett and Bernstein found no significant coherence between moorings separated by distances of 50 km or more. This result is consistent with all the estimates of λ_h reported in this work and supports third-order modal dominance of the observed internal tide. There were no moorings for separation distances in the range 5.2–50 km.

Hendry (1977) has reported an analysis of the semi-diurnal tide based on observations in the North Atlantic during the Mid-Ocean Dynamics Experiment. He finds that the first baroclinic mode is dominant in the internal semi-diurnal tide. The calculated and observed horizontal wavelengths corresponding to the first mode are 160 km. The internal tide appears to be generated near the Blake Escarpment 700 km from the observational area. Our results and those of Barnett and Bernstein (1975) appear to be inconsistent with Hendry's. However, given the uniqueness of the Blake Escarpment, the generation and characteristics of internal tides observed in the central North Pacific may be quite different from those observed by Hendry.

Additional reports of open ocean measurements of the internal tide are comparatively rare in the literature (Wunsch, 1975). The amplitude of the semi-diurnal internal tide observed during POLE is about 10 m. This value agrees well with similar observations off the California continental shelf (Lee, 1961; Reid, 1956; Summers and Emery, 1963). Mid-Atlantic observations (Seiwell, 1942) show much smaller semi-diurnal internal wave amplitudes, as small as 2.2 m. Observations by Weston and Reay (1969) made during southwest approaches to Britain have amplitudes 5–6 m higher than those presently reported. More observations are required before an adequate description of the semi-diurnal internal tide can be made.

7. Comparison with theory

The local response of the well-mixed layer to a transient wind stress is discussed theoretically by Pollard *et al.* (1973). The PRT model predicts that, after one-half pendulum day, deepening is arrested at a depth $h_{\max}$ given by

$$h_{\max} \approx \frac{2^{3/4}U_*}{(Nf)^{1/2}}, \tag{7.1}$$

where U_* is the friction velocity, f the Coriolis parameter and N the buoyancy frequency of the stably stratified fluid below the well-mixed layer, not including the step in stratification at the base. The mixed-layer depths observed during POLE are typically two to three times greater than those predicted by the PRT model. This suggests that entrainment at the base of the mixed layer, due to the shear of the mean flow, was insignificant during the POLE Experiment. This result is consistent with velocity measurements made during the experiment (Davis *et al.*, 1978). They found that, at frequencies below 0.05 Hz, the currents at all levels above 135 m were highly coherent, nearly parallel and of similar magnitude. The velocity measurements imply little shear available to erode the base of the mixed layer as required by the PRT model.

Niiler (1975) suggests that for steady, positive, surface heating and wind stress, deepening is arrested at a depth

$$h_{\max} \approx 2m_0\left(\frac{\tau_0}{\rho_0}\right)^{3/2}\rho_0 c_p/\beta g Q_0, \tag{7.2}$$

where Q_0 is the surface heat flux, c_p the specific heat of sea water, β the thermal coefficient of expansion of sea water and g the acceleration due to gravity. The constant m_0 is related to the Kraus-turner constant m through the relation $m = (c_{10}\rho_a/\rho_0)^{1/2}m_0$, where c_{10} is the drag coefficient at 10 m, ρ_a and ρ_0 are the densities of air and water, respectively. For values of Q_0 greater than a few mW cm^{-2}, the predicted values of $h_{\max}$, with $m = 0.0012$, underestimate the observed mixed-layer depths by about a factor of 2. This implies the assumed value of m is too small by a similar factor.

The theory of the seasonal thermocline advanced by Kraus and Turner (1967) assumes that the turbulent energy available for mixing is some constant fraction m of the downward transfer of energy from the local wind field. Through entrainment, this energy is used to raise the potential energy of the water column. Since the salinity did not contribute significantly to the observed density structure during POLE, the potential energy may be calculated by the method of Turner (1969). A mixing event 370 h into the experiment was chosen since it was least likely to be affected by horizontal advection. Analysis for this event yields a value of $m = 0.0017$, in fair agreement with the value $m = 0.0012$ observed by Denman (1973a,b).

Considerable disagreement exists in the reported values of m. Perhaps m is not a constant but rather a function of local oceanic conditions. The possibility of high-energy inertial oscillations in the

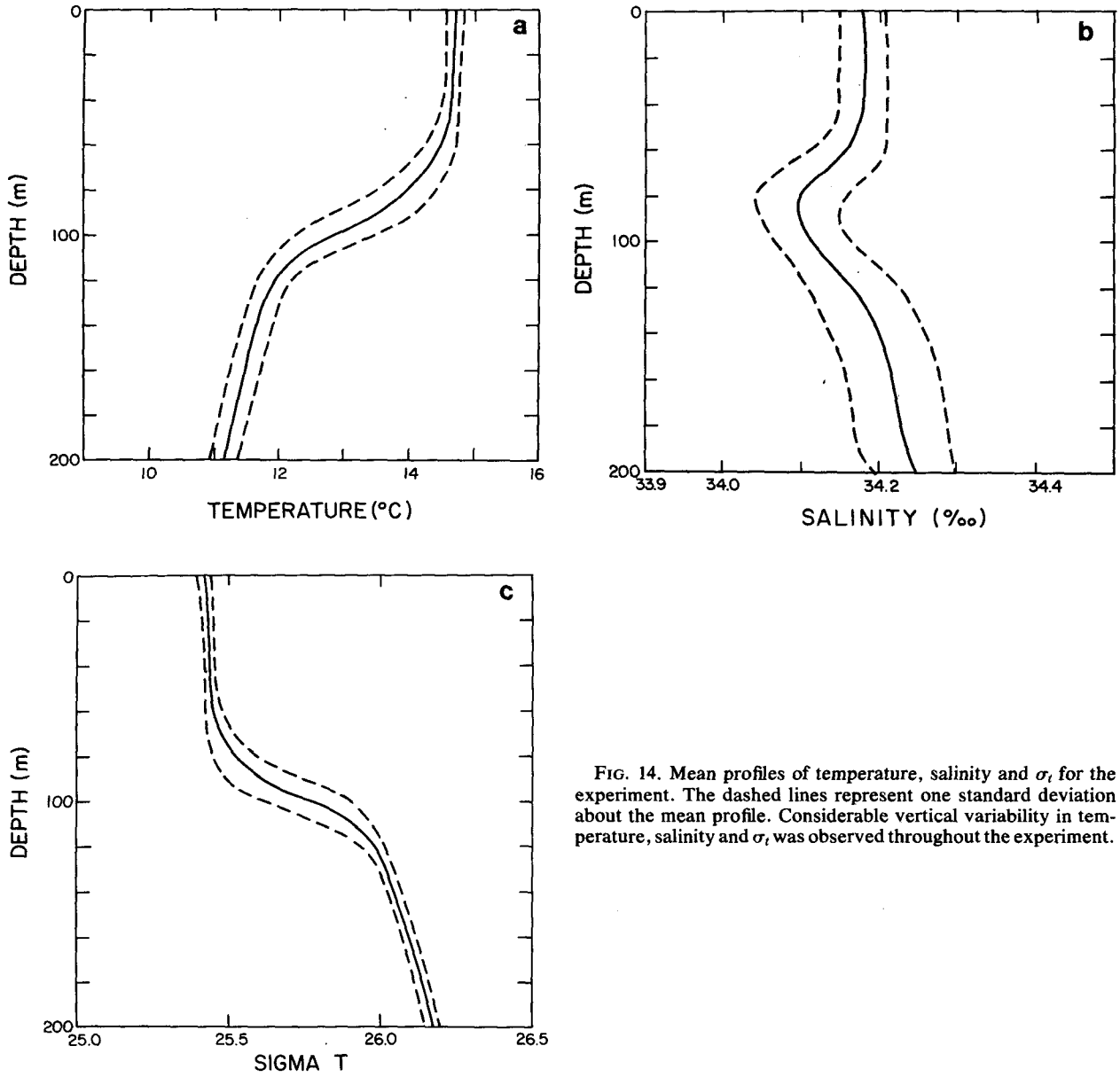

FIG. 14. Mean profiles of temperature, salinity and σ_t for the experiment. The dashed lines represent one standard deviation about the mean profile. Considerable vertical variability in temperature, salinity and σ_t was observed throughout the experiment.

mixed layer at the time of observations reported by Turner (1969) may partially explain the order-of-magnitude discrepancy in the reported values of m.

8. Advection

Mean profiles of temperature, salinity and σ_t, based on all the STD casts taken during the experiment, are shown in Fig. 14. Departures from the mean, calculated as one standard deviation from the mean, are represented by the dashed lines in the figure. The data suggest that considerable variation occurred in the vertical distribution of temperature, salinity and density observed during the experiment. A mean T-S diagram for the upper 200 m, together with standard deviation, is shown in Fig. 15. Several features are immediately evident from these figures. The high temperature and salinity of the surface waters are representative of the Eastern North Pacific Central Water characteristically found near 35°N. This water mass must be distinguished from the larger Western North Pacific Central Water mass. (Sverdrup *et al.*, 1942). The shallow salinity minimum in the figure is characteristic of the eastern North Pacific (Reid, 1973; Kenyon, 1978) and extends southward to the equator. This salinity minimum should be distinguished from the minimum associated with North Pacific Intermediate Water which occurs at greater depths. This Intermediate Water is present below the

central water masses all over the North Pacific. Below the Intermediate Water, the salinity increases regularly. Here Pacific Common Water is found.

Individual hydrocasts taken throughout the experiment are shown in Fig. 16. They show the frequent presence of salinity-compensated temperature inversions at the base of the upper layer and suggest that horizontal advection, variable with depth, is relevant to a complete understanding of the observed structure. The salinity maxima shown in the figure can be associated with the Subtropical Water Mass formed in the trade winds region northeast of the Hawaiian Island Chain where the flux of latent heat typically exceeds 9.8 mW cm^{-2} over a 24 h period (Wyrtki, 1965). The intermittent lateral interleaving of this water mass is characteristic of observations made during the POLE Experiment and may partially explain the failure of one-dimensional mixed-layer deepening theories to properly model the observed mixed-layer depths and surface temperatures.

An estimate of the horizontal temperature gradient can be made from the vertically integrated conservation of heat equation

$$\frac{\partial H}{\partial t} + \nabla\cdot(\mathbf{U}H) + \nabla\cdot(\nabla AH) = Q, \qquad (8.1)$$

where $\partial H/\partial t$ is the local rate of change of heat content H, $\nabla\cdot(\mathbf{U}H)$ is the horizontal divergence of the heat flux, due to advective processes associated with ocean current $\mathbf{U}$, $\nabla\cdot(\nabla AH)$ is the divergence of heat flux, both horizontal and vertical, associated with mixing processes, characterized by an Austauch coefficient A, and Q is the total heat flux due to turbulent and radiative transfer processes at the air-sea interface.

Vertical motions at the base of the vertically integrated layer are neglected. Mixing processes of the form $\nabla\cdot(\nabla AH)$ may reasonably be neglected for time scales of a few hours. The air-sea heat exchange processes were measured directly and the local change in heat content was calculated from the observed temperature profiles. The second term in Eq. (8.1) was calculated as the residual of the remaining terms. Current meter observations (Davis *et al.*, 1978) suggest typical velocities past *Flip* (i.e., relative currents) are of the order 1 to 10 cm s^{-1}. These results lead to temperature gradients of the order ± 0.1 to ± 0.01°C km^{-1}.

Errors associated with the total surface heat flux are about $\pm 10\%$. The vertically integrated changes in heat content are within the stated accuracies of the observed temperature profiles ($\pm 5\%$). The most serious error in the estimate of the horizontal temperature gradient may be the neglect of vertical advection at the base of the vertically integrated layer. These errors, coupled with errors in the current meter observations, suggest that the above estimate of horizontal temperature gradient is accurate only to within an order of magnitude.

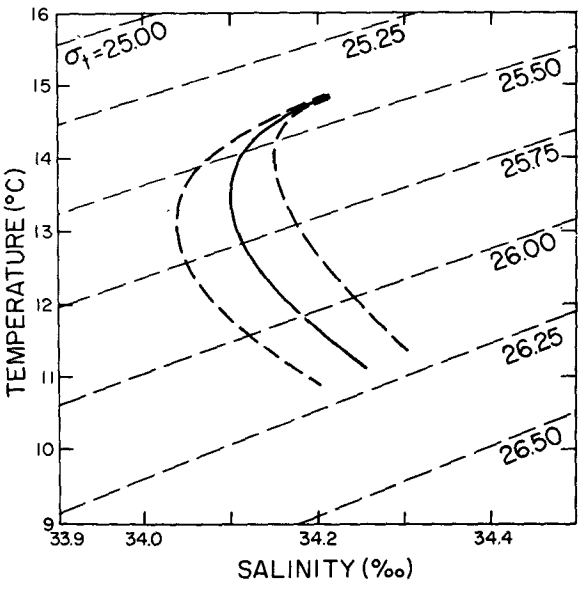

FIG. 15. A mean T-S diagram, constructed from all the profiles. The dashed line represents one standard deviation about the mean. The eastern North Pacific Central Water is evidenced by the high temperatures and salinities of the surface layer. The shallow salinity minimum is characteristic of the eastern North Pacific and should be distinguished from the salinity minimum associated with North Pacific Intermediate Water which occurs at greater depth.

Our estimates of horizontal temperature gradients can be compared with the analysis of XBT, AXBT and STD observations during POLE by Barnett *et al.* (1977). They found that the average near-surface (0–50 m) horizontal temperature gradient over a region 400 km in diameter was 0.005 °C km^{-1}. Superimposed on the mean field were fluctuations having a standard deviation of 0.4 °C about the mean. Approximately half of the variability was associated with horizontal scales of less than 50 km. Taking 0.2°C (25 km)$^{-1}$ = 0.008°C km^{-1} we obtain an estimate of the characteristic temperature gradient associated with small-scale variability. When this gradient is added to the mean gradient, the estimate of local gradients falls within the range we estimated from our observations.

9. Conclusion

Analysis of 15 days of intensive STD profiling from *R/P Flip* as part of the NORPAX POLE Experiment yields the following results:

1) Autocorrelations for the time series of depth of several σ_t surfaces confirm the presence of a semi-diurnal internal tide in the observed records.

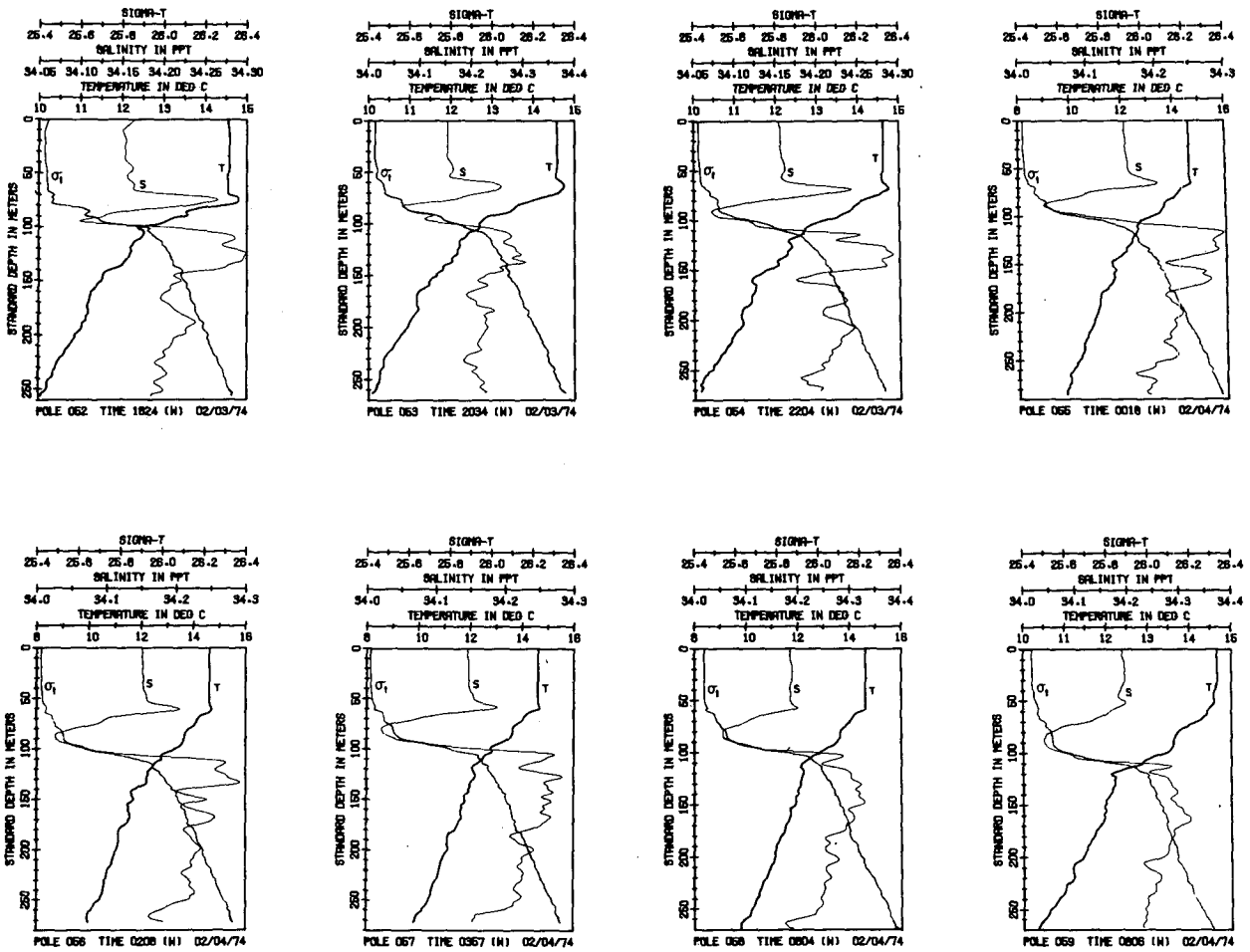

FIG. 16. Individual profiles of temperature, salinity and σ_t taken during the experiment. The salinity maxima frequently occurring at depth suggests horizontal advection of the Subtropical Water mass formed in the evaporative basin northeast of Hawaii.

The period of 12.7 h determined from the autocorrelation analysis is not statistically significantly different from the 12.4 h period of the M2 semi-diurnal tide.

2) The amplitude of the semi-diurnal internal tide is about 10 m and agrees with other observations in the Pacific.

3) The coherence between all pairs of time series of the depth of σ_t surfaces is high, ranging from 0.97 to 0.91. The peak in the coherence spectrum corresponds to a period of 11.6 h, close to the M2 semi-diurnal tidal period. Energy from the semi-diurnal tide is smeared into the next highest frequency band. The limited length of the records prevents finer spectral resolution in the frequency domain.

4) The coherence between a given σ_t surface and deeper lying surfaces decreases slowly with the mean separation between surface. An estimate of the vertical wavelength λ_v of the semi-diurnal internal tide obtained from the coherence vs mean separation data is 1 km.

5) The vertical coherence scale suggests that most of the energy of the semi-diurnal tide is in the third-order modes.

6) For a given σ_t surface, deeper-lying surfaces lag the given surface in time by an amount dependent on the mean separation between surfaces. The data suggest that the phase difference increases with separation at the approximate rate of $+35°\ (100\ \text{m})^{-1}$. Deeper lying surfaces lagging shallower surfaces is consistent with the suggestion that energy is being propagated vertically upward. An estimate of the vertical wavelength λ_v from the phase data is 1.2 km.

7) An estimate of the horizontal wavelength of the semi-diurnal internal tide calculated from the measured buoyancy frequency and the dispersion relation for internal waves under the assumptions of a linear density gradient and the Boussinesq approximation is $30 \leq \lambda_h \leq 35$ km. Affects of rotation were neglected but can effect the estimate by no more than 20%.

8) The observations of the semi-diurnal internal tide presently reported are consistent with those re-

ported by Barnett and Bernstein (1975) based on temperature observations made from moorings in the central North Pacific. Our results and those of Barnett and Bernstein (1975) appear to be inconsistent with those of Hendry (1977).

9) One-dimensional mixed-layer deepening models failed to predict the mixed-layer depths and temperatures observed during POLE. Horizontal advection, as evidenced from the salinity maximum frequently occurring at the bottom of the mixed layer and other near-surface changes in salinity and temperature unassociated with local surface forcing, are responsible for the failure.

10) For the one mixing event in which the possible effects of horizontal advection could be ignored, a value of the mixing energy-flux coefficient $m = 0.0017$ was obtained. This is in fair agreement with the value of 0.0012 reported by Denman.

11) Estimates of the local temperature gradient calculated as the residual in the conservation of heat equation from measurements of the surface heat flux and vertical temperature structure are within the range $0.1-0.01°C\ km^{-1}$. These values are consistent with similar estimates made by Barnett *et al.* (1977) using XBT, ABXT and STD observations.

Acknowledgments. This research was supported by the Office of Naval Research through Contract N0014-76-C-0067 under project NR 083-102. The cooperation of the officers and crew of the *R/P Flip* and the assistance of Alan Lillich in the analysis is gratefully acknowledged. Some of the computations were carried out at the computer facility of the National Center for Atmospheric Research which is sponsored by the National Science Foundation. The authors wish to thank Dr. R. A. de Szoeke for his helpful comments during the preparation of the manuscript. The constructive suggestions of the two anonymous reviewers and the typing skills of Sue Watt, Ruth Ebey and Ruth Hill are gratefully acknowledged. The MLRG graphics department, under the direction of Fred Crowe, prepared the figures.

REFERENCES

Barnett, T. P., 1976: Large scale variation of the temperature field in the North Pacific Ocean. *Naval Res. Rev.*, March, 36–51.

——, and R. L. Bernstein, 1975: Horizontal scales of midocean internal tides. *J. Geophys. Res.*, **80**, 1962–1964.

——, R. A. Knox and R. A. Weller, 1977: Space/time structure of the near-surface temperature field during the NORPAX POLE Experiment. *J. Phys. Oceanogr.*, **7**, 572–579.

Bronson, E. D., and E. R. Glosten, 1968: Floating instrument platform. Scripps Inst. Oceanogr., Univ. Calif., Mar. Phys. Lab. Tech. Rep., SIO Ref. 62–64, 23 pp.

Davis, R., T. P. Barnett and C. S. Cox, 1978: Variability of near-surface currents observed during the POLE Experiment. *J. Phys. Oceanogr.*, **8**, 290–301.

Defant, A., 1961: *Physical Oceanography*, Vols. 1 and 2. Pergamon Press, 729 pp., 598 pp.

Denman, K. L., 1973a: A time-dependent model of the upper ocean. *J. Phys. Oceanogr.*, **3**, 173–184.

——, 1973b: Energy changes associated with wind mixing in the upper ocean. *Fish. Res. Bd. Can. Tech. Rep.*, No. 380, 15 pp.

Dorrestein, R., 1979: On the vertical buoyancy flux below the sea surface as induced by atmospheric factors. *J. Phys. Oceanogr.*, **9**, 229–231.

Elliot, G. W., 1975: Automatic processing system for oceanographic data from U.S. B-scale ships in GATE. *STD Conference and Proceedings*, Plessey Environmental Systems, 163–175.

Fofonoff, N. P., and S. Tabata, 1958: Program for oceanographic computations and data processing on the electronic digital computer ALWAC III-E, DP-1 oceanographic station data program. *Fish. Res. Bd. Can. Ms. Rep. Ser.* (Oceanographic and Limnological), No. 25, 33 pp.

Friehe, C. A., and K. F. Schmitt, 1974: Estimates of surface heat fluxes during POLE. *NORPAX Highlights*, **2**, 8–9.

——, 1976: Parameterization of air-sea interface fluxes of sensible heat and moisture by bulk aerodynamic formulas. *J. Phys. Oceanogr.*, **6**, 801–809.

Hendry, R. M., 1977: Observations of the semi-diurnal internal tide in the western North Atlantic Ocean. *Phil. Trans. Roy. Soc. London*, **A286**, 1–24.

Holland, J. Z., 1968: An application of some statistical techniques to study eddy structure. U.S. Atomic Energy Commission, Div. Tech. Inform., Tech. Rep. No. TID-24585, 340–350.

Kenyon, K. E., 1978: The shallow salinity minimum of the eastern North Pacific in winter. *J. Phys. Oceanogr.*, **8**, 1061–1069.

Kraus, E. B., and J. S. Turner, 1967: A one-dimensional model of the seasonal thermocline—II. The general theory and its consequences. *Tellus*, **19**, 98–106.

Lee, O. S., 1961: Observations of internal waves in shallow water. *Limnol. Oceanogr.*, **6**, 3.2–321.

Mosetti, F., 1967: A new formula for the connection of seawater conductivity with salinity and temperature. *Boll. Geofis. Teor. Appl.*, **8**, 213–217.

Niiler, P. P., 1975: Deepening of the wind-mixed layer. *J. Mar. Res.*, **33**, 405–427.

Paulson, C. A., and J. J. Simpson, 1977: Irradiance measurements in the upper ocean. *J. Phys. Oceanogr.*, **7**, 952–956.

Pollard, R. T., P. B. Rhines and R. O. R. Y. Thompson, 1973: The deepening of the wind mixed layer. *Geophys. Fluid Dyn.*, **3**, 381–404.

Reid, J. L., 1956: Observations of internal tides in October. *Trans. Amer. Geophys. Union*, **37**, 278–289.

——, 1965: Intermediate waters of the Pacific Ocean. *Johns Hopkins Oceanogr. Stud.*, **2**, 85 pp.

——, 1973: The shallow salinity minimum of the Pacific Ocean. *Deep-Sea Res.*, **20**, 51–68.

Roden, G. I., 1970: Aspects of the mid-Pacific transition zone. *J. Geophys. Res.*, **75**, 1097–1109.

——, 1972: Temperature and salinity fronts at the boundaries of the subarctic-subtropical transition zone in the western Pacific. *J. Geophys. Res.*, **77**, 7155–7187.

——, 1974: Thermohaline structure, fronts and sea-air energy exchange of the trade wind region east of Hawaii. *J. Phys. Oceanogr.*, **4**, 168–182.

Seckel, G., 1968: A time sequence oceanographic investigation in the North Pacific trade wind zone. *Trans. Amer. Geophys. Union*, **49**, 377–386.

Siewell, H. R., 1942: An analysis of vertical oscillations in the southern North Atlantic. *Proc. Amer. Phil. Soc.*, **85**, 136–158.

Simpson, J. J., 1977: Small scale temperature structure of the upper ocean. Ph.D. dissertation, Oregon State University, 148 pp.

——, and C. A. Paulson, 1977: Mixed layer observations during the NORPAX POLE Experiment: A data report. Oregon State Univ., Data Rep. 66, Ref. 77–6, 167 p.

——, and ——, 1979a: Mid-ocean observations of atmospheric radiation. *Quart. J. Roy. Meteor. Soc.*, **105**, 487–502.

——, and ——, 1979b: The spectrum of sea surface temperature. *J. Phys. Oceanogr.* (to be submitted).

Sverdrup, H. U., M. W. Johnson and R. H. Fleming, 1942: *The Oceans: Their Physics, Chemistry, and General Biology*. Prentice-Hall, 1087 pp.

Summers, H. J., and K. O. Emery, 1963: Internal waves of tidal period of Southern California. *J. Geophys. Res.*, **68**, 827–839.

Sweers, H. E., 1971: A comparison of methods used to calculate sigma-*t*, specific volume anomaly and dynamic height. *Mar. Tech. Soc. J.*, **5**, 7–26.

Turner, J. S., 1969: A note on wind mixing at the seasonal thermocline. *Deep-Sea Res.*, **16**, 297–300.

——, 1973: *Buoyancy Effects in Fluids*. Cambridge University Press, 367 pp.

Weston, D. E., and W. W. Reay, 1969: Tidal period internal waves in a tidal stream. *Deep-Sea Res.*, **16**, 473–478.

Wunsch, C., 1975: Internal tides in the Ocean. *Rev. Geophys. Space Phys.*, **13**, 167–180.

Wyrtki, K., 1965: The average annual heat balance of the North Pacific Ocean and its relation to ocean circulation. *J. Geophys. Res.*, **70**, 4547–4559.